Stable and Unstable Evolution of Modons Perturbed by Surface Term, Bottom Friction, and Bottom Topography Incorporating Nonlinear Ekman Pumping

BENKUI TAN

Laboratory for Severe Storm Research, Department of Atmospheric Sciences, Peking University, Beijing, China

JOHN P. BOYD

Department of Atmospheric, Oceanic and Space Sciences, University of Michigan, Ann Arbor, Michigan

(Manuscript received 25 July 2002, in final form 12 August 2003)

ABSTRACT

The evolution, both stable and unstable, of contrarotating vortex pairs (''modons'') perturbed by upper-surface and bottom Ekman pumping is investigated using a homogeneous model with a variable free upper-surface and bottom topography. The Ekman pumping considered here differs from the classical Ekman pumping in that the divergence-vorticity term in the vorticity equation, nonlinear and omitted in previous studies, is explicitly included. Under the influence of both nonlinear Ekman pumping and the beta term, eastward- and westward-moving modons behave very differently.

Eastward-moving modons are stable to the upper-surface perturbation but westward-moving modons are not. The latter move southwestward, triggering the tilt instability: the beta effect deepens the cyclones but weakens the anticyclone, and the vortex pair disperses into wave packets.

Eastward-moving modons are stable to bottom friction in the sense that they diminish in time gradually at a rate independent of the signs of the vortices. Westward-moving modons behave differently depending on the strength of bottom friction. Cyclones decay faster than anticyclones, triggering the tilt instability in westward-moving modons, but only if the bottom friction is very weak. For sufficiently strong bottom friction, in contrast, modons decay monotonically: the cyclones still decay faster than anticyclones, but no wave packets formed before the modons completely dissipate.

Westward-moving modons are *always* unstable to topographic forcing. Eastward-moving modons have varying behavior controlled by the height and width of the topography. Below a critical height, determined by the width, modons survive the topographic interaction: their trajectory meanders but the two contrarotating vortices always remain bound together after escaping the topography. Above the critical height, modons disassociate: the two vortices separate and disperse into wave packets. When the width of the topography is comparable to modon width, there exists a stable window within the unstable region of the topographic height in which the modons also survive the topographic encounter.

1. Introduction

Since the pioneering work by Larichev and Reznik (1976), vortex pairs known as modons have attracted a great deal of attention because of their potential applications, in both geophysical fluid dynamics and in plasma physics. Modons are solutions to the partial differential equation called the ''quasigeostrophic equivalent barotropic vorticity equation'' in geophysics and the ''Hasegawa–Mima equation'' in plasma physics. In plasma physics, it is believed that the modons may be important for understanding anomalous transport across the magnetic flux surface (Hesthaven et al. 1993). In geophysical fluid dynamics, modon theory is used for an explanation of the atmospheric blocking phenomenon (McWilliams 1980; Butchart et al. 1989). The modon theory is also possibly connected to the dipole vortex generation in laboratory experiments (Nezlin and Snezhkin 1993).

Modon stability is obviously an important issue in all modon applications. Gordin and Petviashvili (1985), Laedke and Spatschek (1986), Sakuma and Ghil (1990), and Swaters (1986a) concluded that the modon solution is stable. However, Nycander (1992) proved that all earlier ''proofs'' above are insufficient; the stability problem is still mathematically unsolved.

Numerically, McWilliams et al. (1981), McWilliams and Zabusky (1982), and Zabusky and McWilliams (1982) showed that both eastward- and westward-propagating modons can survive a wide variety of finite perturbations, so modons are rather stable. Nevertheless, Makino et al. (1981) showed that an eastward-traveling

Corresponding author address: Dr. Benkui Tan, Laboratory for Severe Storm Research, Department of Atmospheric Sciences, Peking University, Beijing 100871, China.
E-mail: bktan@pku.edu.cn

modon behaves quite differently from a westward-traveling modon when the axis connecting the centers of the two vortices, usually north–south, is tilted. The trajectory of a tilted eastward-traveling modon is gently oscillatory while a tilted westward-traveling modon executes a cycloidal motion with large excursions from the initial direction of propagation. The later phenomenon is now called the tilt instability. The difference in modon behavior can be explained by conservation of potential vorticity. For the eastward-traveling case, the inhomogeneous term, βy, reduces the relative vorticity ς_g when the modon moves in the meridional direction, so the tilted modon wobbles and its trajectory oscillates gently around its initial latitude. For the westward-traveling case, the inhomogeneous term enhances ς_g, so the tilted modon changes its structure and velocity (''tilt instability'') rapidly. Later, Hobson (1991) and Hesthaven et al. (1993) numerically studied the tilt instability with a perturbation of propagation of arbitrary amplitude in the initial direction. Tilted modons, whether initially traveling eastward or westward, either end up propagating eastward with a damped meridional oscillation or disintegrate, depending on their initial tilting angle and intensity.

This tilt instability is confirmed theoretically, using a method of multiple expansion, by Araki et al. (1998), who showed that the tilted modons are structurally unstable regardless of the direction of propagation. Wu and Mu (1999) also showed by a Lyapunov functional method that modons are nonlinearly unstable.

In the above studies, the axial tilts were imposed on the initial conditions. In reality, modons are perturbed by various physical processes. How modons react to these physical perturbations is an interesting problem. Swaters (1986b), Carnevale et al. (1988a) and Carnevale et al. (1988b) examined the influence of bottom topography on eastward-moving modons analytically and numerically. Swaters (1986b) chose the topography to be a slowly varying ridge and developed a Wentzel–Kramers–Brition (WKB) approximation. He found that as the modon moves into deeper (shallower) fluid, the modon translational speed increases (decreases), and the modon radius decreases (increases). Carnevale et al. (1988a,b) chose topography of various shapes with arbitrary amplitude. They found numerically that modons either survive the topographic forcing or break down, depending on the topographic and the initial modon parameters.

Parenthetically, note that there have also been studies of the interaction of a single vortex (''monopole'') with topography as in Zavala Sansón et al. (1999) and other articles they reference. However, because the two contrarotating vortices in a modon are strongly coupled, the topographic interactions of a single vortex with topography are but an imperfect guide to those of a modon.

McWilliams et al. (1981), Swaters (1985, 1989), and Swaters and Flierl (1989) studied, numerically and/or analytically, the damping of modons due to bottom boundary layer friction. Dissipation causes modon amplitudes to diminish in time regardless of their directions of propagation. In addition, an eastward-moving modon slows and then *reverses* its direction of propagation.

In plasma physics, Jovanovic and Horton (1993) studied the stability of drift-wave modons in the presence of temperature gradients using Lyapunov's functional method. They concluded that the dipole vortex structure is more stable in the presence of a finite-temperature gradient than was previously thought. In the same paper, they also numerically investigated modon stability in the presence of monopole and dipole perturbations and found that vortices propagating in the direction of the electron diamagnetic drift, or a westward geophysical vortex, are tilt unstable with exponential growth of the initial tilt and splitting of the vortex.

In this paper, we systematically study the effects on modons of an upper boundary layer with a moving free surface, which has not been studied before, and a lower boundary layer with a variable bottom. In our paper, the nonlinear divergence-vorticity term in the vorticity equation, omitted in previous studies, will be included. The Ekman pumping considered here, therefore, is nonlinear, and it turns out that this nonlinear Ekman pumping along with the beta effect is very significant in modon dynamics. It usually results in dramatic differences between eastward- and westward-moving modons. Perturbed by the surface term, eastward-moving modons are little changed, but westward-moving modons first move southwestward and then display the tilt instability.

In presence of bottom friction induced by the nonlinear Ekman pumping, eastward-moving modons are still similar to those of McWilliams et al. (1981), Swaters (1985, 1989), and Swaters and Flierl (1989). In contrast, westward-moving modons decay assymetrically with cyclones dying out much faster than anticyclones. Because of this asymmetrical decay, westward-moving modons deviate from their initial due-westward propagation and veer northwestward. This enhances the asymmetry in the strength of the two vortices (due to the beta effect) to trigger the tilt instability; the modons finally evolve into wave packets. This sort of evolution was emphatically *not* observed in McWilliams et al. (1981), Swaters (1985, 1989), and Swaters and Flierl (1989).

Our work shows that by using a simple form of bottom topography—a ridge—topographic effects on modons are very complex depending on both the direction of propagation and the topographic parameters. Westward-moving modons are always unstable to topographic interaction. For eastward-moving modons, behavior is a function of both the height and the width of the topography. The ridge width determines a critical height. Below this, modons survive propagation over topography: their trajectories meander but the vortices never disassociate. When the ridge is taller than the critical height, modons break down: their two vortices separate and disperse into wave packets. When the width

of the topography is comparable to the modon width, there exists a stable window in the unstable interval of topographic height in which the modons also survive the topographic forcing. Our work here differs from Carnevale et al. (1998b), as explained more fully in sections 4 and 5.

The effects of the upper-surface perturbation, bottom friction, and topographic forcing on modons will be explored fully in this work, either separately or combined. Our paper is organized as follows. In the next section, the governing equation is derived and the pseudospectral numerical algorithm is briefly described. In section 3, three typical kinds of unstable evolution of tilted westward-moving modons and the asymmetrical vortex decay are illustrated. Section 4 reports numerical results for modons under the influence of the upper-surface perturbation, bottom friction, and topographic forcing. Finally the main conclusions are summarized in section 5.

2. The model and the governing equation

The model here is an incompressible homogeneous fluid on an infinite beta plane with a free surface $h(x, y, t)$ as its upper boundary and a variable bottom $h_B(x, y)$ as its lower boundary. The flow is divided vertically into three layers: the upper boundary layer, the interior, and the lower boundary layer. Friction is important in the upper and lower boundary layers, but is neglected in the interior. The flow is in hydrostatic balance, so the pressure gradient force is independent of height and proportional to the free surface. The horizontal momentum equations of motion in the interior are

$$\frac{\partial u}{\partial t} + u\frac{\partial u}{\partial x} + v\frac{\partial u}{\partial y} - fv = -g\frac{\partial h}{\partial x},$$
$$\frac{\partial v}{\partial t} + u\frac{\partial v}{\partial x} + v\frac{\partial v}{\partial y} + fu = -g\frac{\partial h}{\partial y}, \qquad (2.1)$$

where u and v are the east–west and north–south velocities, respectively, which are independent of height, and $f = 2\Omega \sin\varphi$ is the Coriolis parameter.

The vorticity equation under the beta-plane approximation can be obtained by taking the curl of Eq. (2.1):

$$\frac{\partial \varsigma}{\partial t} + u\frac{\partial \varsigma}{\partial x} + v\frac{\partial \varsigma}{\partial y} + \beta_0 v = -(f_0 + \varsigma)\left(\frac{\partial u}{\partial x} + \frac{\partial v}{\partial y}\right), \qquad (2.2)$$

or

$$\frac{\partial \varsigma}{\partial t} + u\frac{\partial \varsigma}{\partial x} + v\frac{\partial \varsigma}{\partial y} + \beta_0 v = (f_0 + \varsigma)\frac{\partial w}{\partial z}, \qquad (2.3)$$

where $\varsigma = \partial v/\partial x - \partial u/\partial y$ is the vertical vorticity, w is the vertical velocity, $f_0 = 2\Omega \sin\varphi_0$ is constant, and $\beta_0 = df/dy =$ constant. Large-scale flow is in quasigeostrophic balance, and the velocities and vorticity in Eq. (2.3) can be approximated by the corresponding geostrophic values:

$$u \approx u_g \equiv -\frac{g}{f_0}\frac{\partial h}{\partial y}, \qquad v \approx v_g \equiv \frac{g}{f_0}\frac{\partial h}{\partial x},$$
$$\varsigma \approx \varsigma_g \equiv \frac{g}{f_0}\left(\frac{\partial^2 h}{\partial x^2} + \frac{\partial^2 h}{\partial y^2}\right). \qquad (2.4)$$

Integrating Eq. (2.3) vertically from the lower boundary of the interior to its upper boundary, and assuming that the depths of the upper and lower boundary layers, and the deviation of the height of the free surface in motion from the height of the free surface in rest, are much smaller than the height of the free surface in rest, yields

$$\frac{\partial \varsigma_g}{\partial t} + u_g\frac{\partial \varsigma_g}{\partial x} + v_g\frac{\partial \varsigma_g}{\partial y} + \beta_0 v_g = \frac{(f_0 + \varsigma_g)}{D}(w_{\text{Top}} - w_{\text{Bottom}}), \qquad (2.5)$$

where D is the height of the free surface when the flow is in rest. The vertical velocity at the boundary separating the upper boundary layer and the interior is denoted by w_{Top}, and it is equal to the Ekman pumping of the upper boundary layer given by (Pedlosky 1987; Tan 2000)

$$w_{\text{Top}} = \frac{d_g h}{dt} + \frac{\mathbf{k}}{f_0\rho}\cdot\nabla\times\boldsymbol{\tau}_S, \qquad (2.6)$$

where $d_g/dt = \partial/\partial t + u_g(\partial/\partial x) + v_g(\partial/\partial y)$, $\mathbf{k}$ is vertical unit vector, ρ the density of the fluid, and $\boldsymbol{\tau}_s$ the surface stress. The first term in Eq. (2.6), $d_g h/dt$, is the so-called free-surface term caused by the motion of the free surface, which differs from its counterpart in the inviscid theory where the vertical velocity at the free surface is given by $dh/dt = \partial h/\partial t + u(\partial h/\partial x) + v(\partial h/\partial y)$ in which the advective velocities u and v are the actual velocity components, not the geostrophic velocities as here (see Tan 2000, for details). Note that, for the viscous homogeneous flow considered here, the surface term

$$\frac{d_g h}{dt} = \frac{\partial h}{\partial t} + u_g\frac{\partial h}{\partial x} + v_g\frac{\partial h}{\partial y} = \frac{\partial h}{\partial t} - \frac{g}{f_0}\frac{\partial h}{\partial y}\frac{\partial h}{\partial x} + \frac{g}{f_0}\frac{\partial h}{\partial x}\frac{\partial h}{\partial y}, = \frac{\partial h}{\partial t}$$

which means that it is only the local change of the free surface that contributes to the surface term. The second term in Eq. (2.6) is the so-called surface stress term caused by the friction in the upper boundary layer. It is equal to the stress exerted by the external field of forcing which will not be in consideration in this paper.

The term w_{Bottom} in Eq. (2.5) is the vertical velocity at the boundary separating the interior and the lower boundary layer, and it is equal to the Ekman pumping of the lower boundary layer given by

$$w_{\text{Bottom}} = \mathbf{V}_g \cdot \nabla h_B + \frac{\mathbf{k}}{f_0 \rho} \cdot \nabla \times \boldsymbol{\tau}_B, \qquad (2.7)$$

where $\boldsymbol{\tau}_B$ is the stress at the bottom. The first term in Eq. (2.7) is the topographic term due to variation of the bottom topography. Note that the velocity in this term is the geostrophic velocity, which differs from its counterpart in the inviscid theory, where the vertical velocity at the bottom is given by $\mathbf{V} \cdot \nabla h_B$ in which the velocity is the actual velocity (see Tan 2000). The second term in Eq. (2.7) is the bottom stress term caused by the friction in the lower boundary layer. To obtain the explicit form of the bottom stress term, some suitable models of stress are required. It is generally a very complicated matter to give explicitly the exact form of the bottom stress term in terms of velocity and/or pressure. However, for an incompressible homogeneous boundary flow, if the stress takes the Newtonian form (Pedlosky 1987) and the viscosity coefficient K is assumed to be a constant, the bottom stress term in Eq. (2.7) is given simply by $\sqrt{(K/2f_0)}\varsigma_g$, which will be used in this paper.

If U, L, L/U, and f_0UL/g are used to denote the scales of the characteristic horizontal velocity, horizontal length, time, and perturbed height of the free surface, the vorticity equation (2.5) can be nondimensionalized as

$$\frac{\partial}{\partial t}(\nabla^2\psi - F\psi) + J(\psi, \nabla^2\psi) + \beta\frac{\partial \psi}{\partial x} = \underbrace{\varepsilon F \nabla^2\psi \frac{\partial \psi}{\partial t}}_{\text{(I)}} \underbrace{- \mu(1 + \varepsilon\nabla^2\psi)\nabla^2\psi}_{\text{(II)}} - \underbrace{(1 + \varepsilon\nabla^2\psi)J(\psi, \eta_B)}_{\text{(III)}}, \qquad (2.8)$$

where the nondimensional parameters are defined as

$$\varepsilon = \frac{U}{f_0 L}, \qquad F = \frac{f_0^2 L^2}{gD}, \qquad \beta = \frac{\beta_0 L^2}{U},$$
$$\mu = \frac{E_k^{1/2}}{\varepsilon}, \qquad E_k = \frac{K}{2f_0 D^2}, \qquad (2.9)$$

and ψ is the nondimensional streamfunction of the interior flow, $\eta_B = h_B/D\varepsilon$ the nondimensional topographic function, and $J(a, b) = (\partial a/\partial x)(\partial b/\partial y) - (\partial a/\partial y)(\partial b/\partial x)$ is the Jacobian operator.

Equation (2.8) is the governing equation that describes the evolution of modons perturbed by the upper and bottom Ekman pumping. Without the terms at the right-hand side, it reduces to the traditional inviscid equivalent barotropic vorticity equation, which possesses the modon solutions given by Eq. (2.10). So the terms on the right-hand side of Eq. (2.8) modify the classical modon. Term I, $\varepsilon F\nabla^2\psi(\partial\psi/\partial t)$, which comes from the convergence-vorticity term in the vorticity equation (2.2) and the variation of the upper free surface, is called here the ''surface perturbation term.'' Terms II and III, $-\mu(1 + \varepsilon\nabla^2\psi)\nabla^2\psi$ and $-(1 + \varepsilon\nabla^2\psi)J(\psi, \eta_B)$, are the perturbations caused by the ''bottom friction term'' and ''topography term,'' respectively. These terms differ from their traditional counterparts by $\mu\varepsilon(\nabla^2\psi)(\nabla^2\psi)$ and $\varepsilon\nabla^2\psi J(\psi, \eta_B)$, which are also closely related to the convergence-vorticity term.

To study the effects of the surface perturbation and the bottom Ekman pumping on modons, Eq. (2.8) is solved numerically in the domain $[-22, 22] \times [-22, 22]$. The spatial discretization is a pseudospectral method with 128×128 Fourier modes; the time-marching scheme is the third-order Adams–Bashforth method (Boyd 2001). As a check, we did some experiments with doubled spatial resolution but found no significant difference from the lower resolution used in most of our calculations. For the numerical experiments where the surface perturbation term $\varepsilon\nabla^2\psi(\partial\psi/\partial t)$ is involved, one must invert a nonlinear operator to obtain an expression for the time derivative $\partial\psi/\partial t$ at each time step. However, the nonlinear inversion can actually be solved easily by using Newton's iteration because ε is small in our problem. In order to suppress the short-wave blocking, an artificial viscosity term $\nu\nabla^6\psi$ with $\nu = 10^{-5}$ is used in all our numerical simulations.

The initial condition is the modon solution (Larichev and Reznik 1976; Flierl et al. 1980), which, in polar coordinates (r, θ), is

$$\psi(r, \theta) = Ac\sin\theta\left[\frac{q^2}{k^2}\frac{J_1(kr/A)}{J_1(kA)} - \frac{r}{A}\left(1 + \frac{q^2}{k^2}\right)\right], \quad r < A,$$
$$\psi(r, \theta) = -Ac\sin\theta\frac{K_1(qr/A)}{K_1(qA)}, \quad r > A, \qquad (2.10)$$

where J_1 and K_1 are the first-order Bessel and modified Bessel functions, respectively; A and c are the core radius and the zonal speed of modons, which are connected to the other parameters through

$$q^2 = A^2\left(F + \frac{\beta}{c}\right), \qquad \frac{K_2(q)}{qK_1(q)} + \frac{J_2(k)}{kJ_1(k)} = 0. \qquad (2.11)$$

The first equation in Eq. (2.11) shows that to be localized (q real), modons can propagate either westward with speed $c < -(\beta/F)$ or eastward with arbitrary speed. The second equation is the dispersion relation for modons, which can be solved for k numerically or analytically (Boyd 1981) when q is given by the first equation.

Our model has four parameters, not including the parameters of the topography described later. It is impossible to fully explore so large a parameter space. In this study, we allow two of them, Rossby number ε and the bottom friction number μ, to vary and the remaining two parameters, the Froude number F and the nondimensional Rossby parameter β, are fixed: $F = 2.0$ and $\beta = 1.0$.

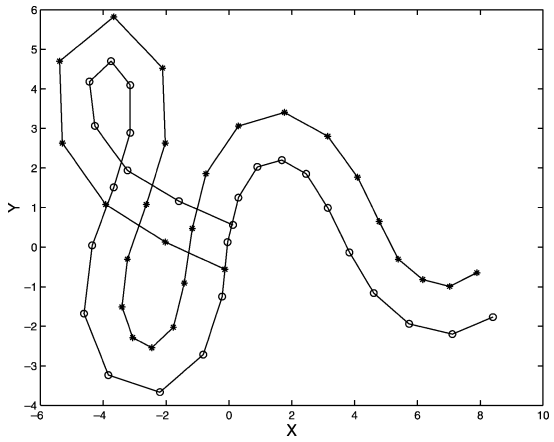

FIG. 1. Unstable evolution of a westward-moving modon tilted initially by an angle of $\pi/10$. Curve with stars (topmost curve on rightside) is the trajectory of the anticyclone and curve with circles is the trajectory of the cyclone. The initial position of the center of the modon is located at $x = 0$. The modon parameters are $A = 1.0$, $c = -1.95$, $q = 1.220$, and $k = 3.955$.

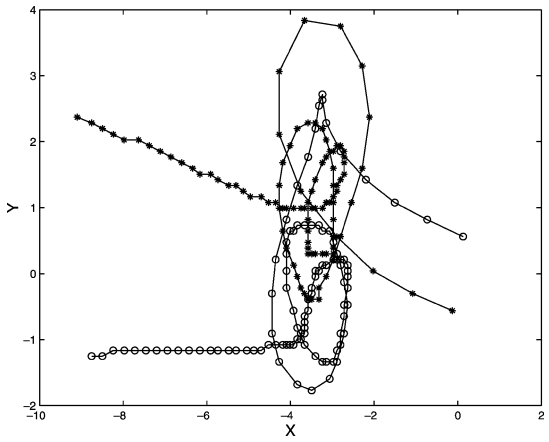

FIG. 2. As in Fig. 1, except the modon parameters are $A = 1.0$, $c = -0.95$, $q = 0.973$, and $k = 3.919$.

3. Some preliminaries

Before we report the numerical simulations on the effects of the upper and bottom Ekman pumping on modons, we first describe the unstable evolution of tilted modons without the perturbations caused by the Ekman pumping and the asymmetrical decay of the vorticity for the fluid parcel subject to the bottom friction through the nonlinear Ekman pumping, which will be very helpful in understanding the simulation results.

a. Unstable evolution of modons suffering tilt instability

In Hobson (1991) and Hesthaven et al. (1993) there are some interesting and detailed studies on the evolution of eastward- and westward-moving modons initially tilted with arbitrary angles. Here, we focus our attention only on the evolution of westward-moving modons initially tilted artificially by a small angle. Our results are obtained by solving Eq. (2.8) without all the terms on the right-hand side and the initial condition is the modon solution Eq. (2.10) tilted by an angle of $\pi/10$.

The tilt instability can evolve in a quite different way depending on the modon amplitude, and there are three typical kinds of evolution (Figs. 1–3). Figure 1 shows the case when the initial amplitude of the modon is relatively large, and the tilt instability makes the modon reverse its direction of propagation from westward to eastward. Initially the modon moves slightly northwestward; as it moves on, the amplitude of the anticyclone increases while the amplitude of the cyclone decreases. Then, the cyclone rotates around the anticyclone from its west side to its east side and the modon moves southward. During its southward motion, the amplitude of the cyclone increases while the amplitude of anticyclone decreases. Then, the anticyclone rotates around the cyclone from its west side to its east side and the modon moves northward again. After repeating this process several times and emitting some of its energy, the modon finally propagates eastward, oscillating around its initial latitude. Figure 2 shows another kind of unstable evolution of a westward-moving modon with medium amplitude. Initially, the modon behaves in a same way as in Fig. 1, then it tumbles very complicatedly for some period of time. Finally, its two vortices separate and move steadily westward until they disperse into wave packets. In Fig. 3, the initial amplitude is small. The modon behaves in a way different from the previous two cases. As the modon moves northward, the amplitude of the anticyclone increases gradually and the amplitude of the cyclone decreases. At the time $t = 12$, the anticyclone becomes the strongest while the cyclone decays to the weakest. Then, the anticyclone begins to disperse downstream into a wave packet: first, a cyclonic eddy is newly formed downstream, then an anticyclonic eddy is gradually established at the right side of the newly established cyclone. In such a way, the wave packet is developed. In the process of its formation, the wave packet is still propagating westward as a whole.

In the later numerical simulations in this paper, we will focus our attention on the modons with smaller amplitudes in order that the nondimensional relative vorticity should be of order unity, which is required by the scale analysis. Indeed we used two sets of parameters: one set of parameters is $A = 1.0$, $c = 0.4$, $k = 2.121$, and $q = 4.091$, which represent an eastward-moving modon; another set of parameters is $A = 1.0$, $c = -0.55$, $k = 3.853$, and $q = 0.4264$, which represent a westward-moving modon. Note that (q, k) are determined by (2.1) as soon as a pair of (a, c) values have been chosen.

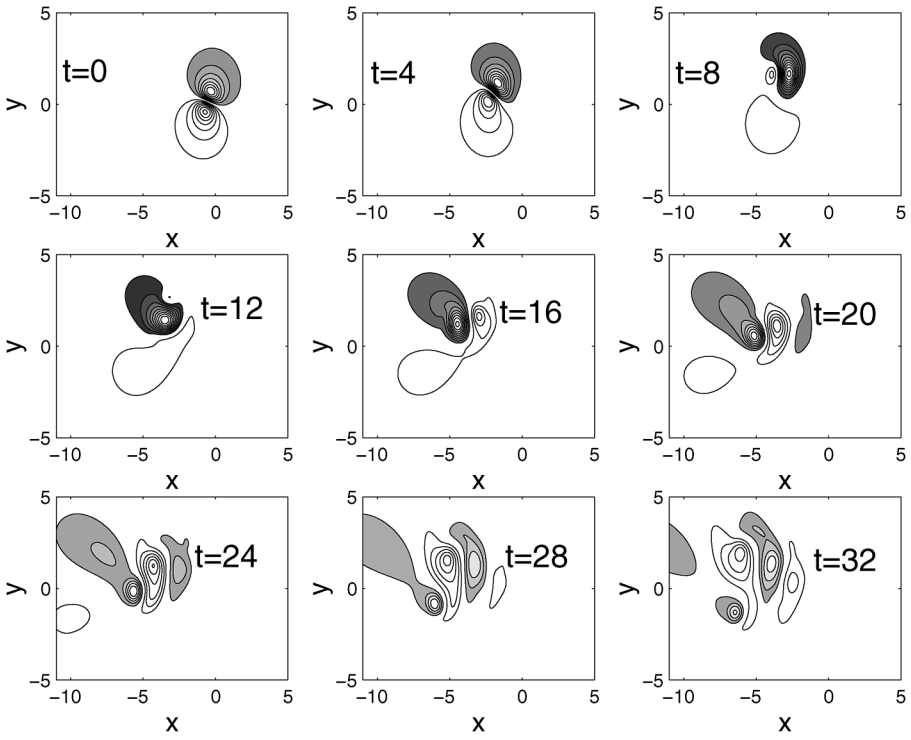

FIG. 3. Unstable evolution of a westward-moving modon tilted initially by an angle of $\pi/10$. Curves in the plot are the contour lines of the modon streamfunction. The interval of the contour lines is 0.1 and the zero contour line has been omitted for clearness. Contour lines are shaded to represent the anticyclone while contour lines with no shading represent the cyclone (the same is true in the following figures). The modon parameters are $A = 1.0$, $c = -0.55$, $q = 0.4264$, and $k = 3.853$.

b. Asymmetrical decay of vorticity of a fluid parcel subject to the nonlinear Ekman pumping

It is well known that the vorticity of a fluid parcel in the free atmosphere subject to bottom friction incorporating classical Ekman pumping will decay exponentially. How the bottom friction incorporating nonlinear Ekman pumping affects the evolution of vorticity of a fluid parcel in the free atmosphere is an interesting problem and is examined here. This is a nonlinear spindown problem on an f plane. For mathematical simplicity, we also set $F = 0$ at the same time. Thus, Eq. (2.8) reduces to

$$\frac{d_g \varsigma_g}{dt} = -\mu(1 + \varepsilon\varsigma_g)\varsigma_g; \tag{3.1}$$

the solution to Eq. (3.1) is (Zavala Sansón and van Heijst 2000)

$$\varsigma_g(t) = \frac{\varsigma_g(0)e^{-\mu t}}{1 + \varepsilon\varsigma_g(0)(1 - e^{-\mu t})}, \tag{3.2}$$

where $\varsigma_g(0)$ is the initial vorticity of the fluid parcel. Clearly, if $\varepsilon = 0$, that is, the divergence-vorticity term is not taken into consideration, the solution (3.2) reduces to the classical spindown solution (Holton 1979):

$$\varsigma_g(t) = \varsigma_g(0)e^{-\mu t}. \tag{3.3}$$

For this case, the vorticity of the fluid parcel decays exponentially, and at the time $t = 1/\mu$, the vorticity of the parcel reduces to about one-third its initial vorticity, whether the vorticity of the parcel is positive or negative. If the divergence-vorticity term is taken into consideration, the solution (3.2) shows that the decay is no longer vorticity symmetric due to the term $\varepsilon\varsigma_g(0)(1 - e^{-\mu t})$ in the denominator in the solution (3.2): the positive vorticity decays faster than in the classical spindown problem while the negative vorticity decays slower than in the classical spindown problem.

4. Numerical results

In this section, we examine the modon evolution perturbed by the surface perturbation, the bottom friction and the topographic forcing, separately and combined.

a. Effects of the surface perturbation

Perturbed by the surface perturbation term, term I at the right-hand side of Eq. (2.8), modons behave differently depending on the initial direction of propagation. Eastward-moving modons are stable to the surface perturbation while westward-moving modons are unstable to the perturbation (see Fig. 4). Initially, the westward-moving modon is perturbed to deviate from its initial east–west direction of propagation and moves south-

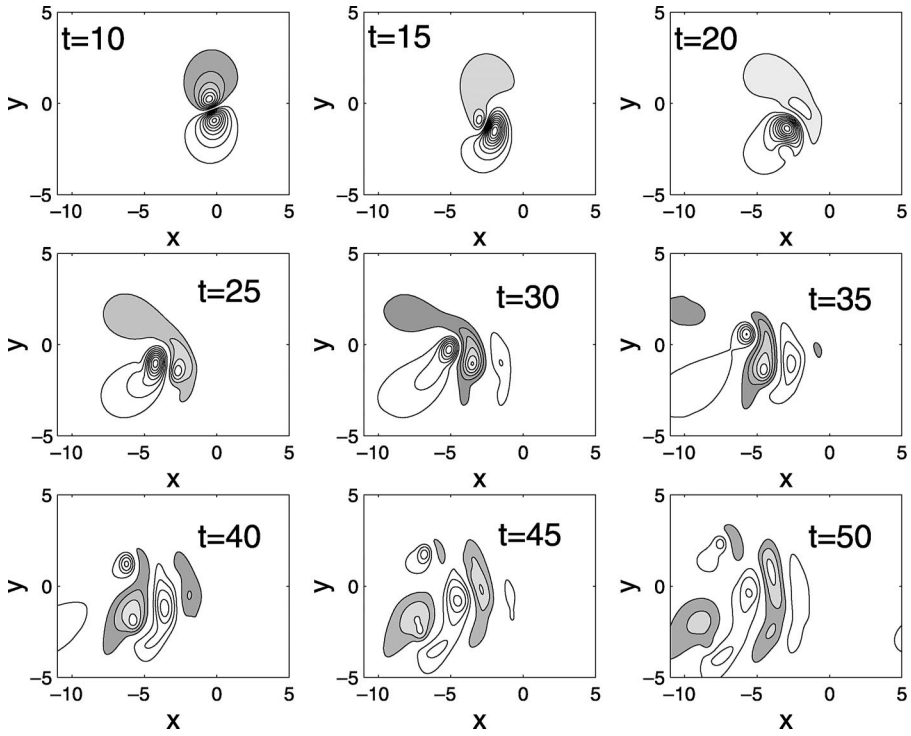

FIG. 4. Unstable evolution of a westward-moving modon perturbed by the upper-surface perturbation with $\varepsilon = 0.05$. The modon parameters are the same as in Fig. 3.

westward. Moving this way, the modon obtains positive vorticity due to the β effect, which deepens its cyclone and weakens its anticyclone, and the weakened anticyclone rotates around the deepened cyclone. At the time $t = 17$, the cyclone becomes stronger while the anticyclone becomes weaker, which has rotated to the left of the cyclone. From that time on, the cyclone begins to disperse downstream into a wave packet: anticyclones and cyclones are gradually developed downstream in an alternative way, propagating westward as a whole.

The time required to trigger the tilt instability depends closely on ε. The smaller the ε is, the longer the time is. For instance, the time at which the cyclone reaches its strongest state is 33 when $\varepsilon = 0.001$; it is 17 when $\varepsilon = 0.05$.

b. Effects of the bottom friction

From the previous section we know that, under the action of the bottom friction incorporating nonlinear Ekman pumping, the vorticity of a fluid parcel on an f plane decays asymmetrically: The positive vorticity decays faster than the negative vorticity. Here we examine the effects of the bottom friction incorporating nonlinear Ekman pumping, term II at the right-hand side of Eq. (2.8), on modons on the β plane.

Under the action of both the beta effect and the bottom friction incorporating nonlinear Ekman pumping, the modon behavior also exhibits asymmetry depending on the initial direction of propagation. For an eastward-moving modon, it is a vortex pair with the cyclone located to the north of the anticyclone. In the presence of the bottom friction incorporating nonlinear Ekman pumping, the modon structure would become asymmetric with a stronger anticyclone and a weaker cyclone due to the asymmetry of decay. With such an asymmetrical structure the modon would deviate from its initial due-eastward direction of propagation and move southeastward. Moving this way it would gain positive voriticity due to the effect of the β term, its cyclone would be enhanced, and its anticyclone would be reduced. So the effect of the beta term counteracts the asymmetrical decay and actually the modon still moves eastward. Its amplitude and velocity diminish in time and finally its direction of propagation is reversed from eastward to westward, as in McWilliams et al. (1981).

For a westward-moving modon, on the other hand, the situation is different. For this case the modon is a vortex pair with the anticyclone located to the north of the cyclone. Under the action of the bottom friction incorporating nonlinear Ekman pumping, the structure of the modon would become asymmetric with a stronger anticyclone and a weaker cyclone due to the asymmetry of decay. With such an asymmetrical structure, the modon would deviate from its initial due-westward direction of propagation and move northwestward. Moving in this direction, the modon would gain negative vorticity due to the β effect. So the difference in the strength

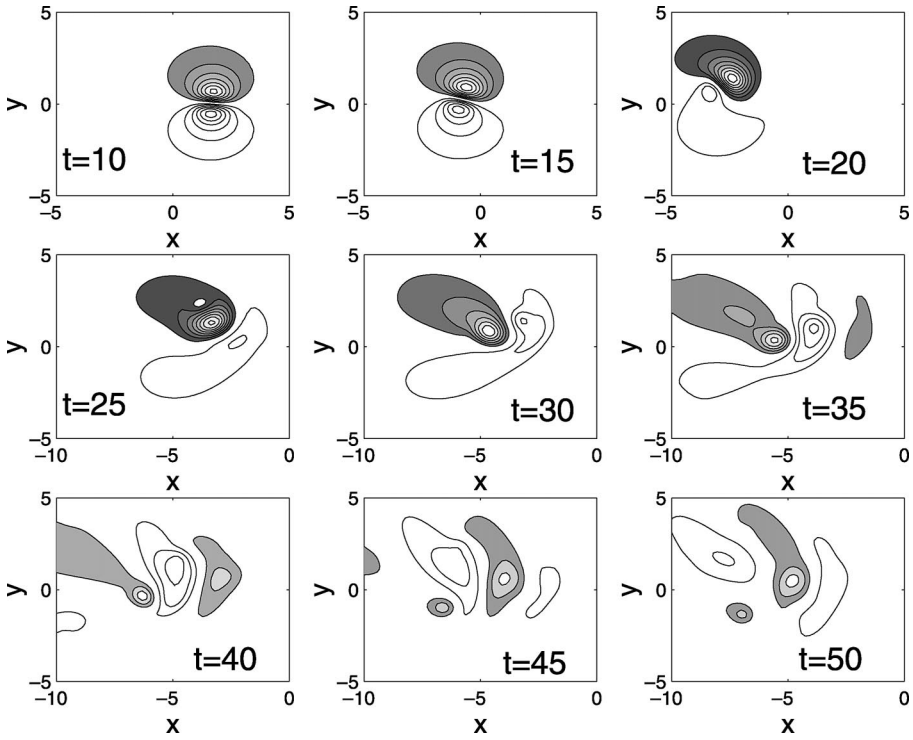

FIG. 5. Unstable evolution of a westward-moving modon subject to bottom friction with $\varepsilon = 0.05$ and $\mu = 0.01$. The modon parameters are as in Fig. 3. The plots are the contour lines of the modon streamfunction.

of the cyclone and anticyclone caused by the bottom friction is further enhanced by the β effect, and the modon actually moves northwestward. After some period of time, the anticyclone reaches it strongest point and the cyclone decays to its weakest point. Then the anticyclone rotates clockwise, disperses its energy rightward, and becomes a wave packet, gradually dying away. Figure 5 shows a typical example for this kind of evolution where $\mu = 0.01$.

When the bottom friction is stronger—see $\mu = 0.05$ in Fig. 6—the modon behaves initially in the same way as in Fig. 5, but it behaves differently in its later stage of evolution. After the time at which the cyclone disappears, the anticyclone decays very rapidly before it disperses fully into a wave packet (Fig. 6).

c. *Effects of the topographic forcing*

This section reports numerical results on the effects of the topographic forcing, term III at the right-hand side of Eq. (2.8), on the modon behavior. The details of the evolution of the modons do depend on the shapes of topography considered. Here, though, we examine only the general characteristics of modons when they move over topography. So we employ only a particular kind of topography: a ridge of form

$$\eta_B(x) = h_0 \operatorname{sech}\left(\frac{x^2}{\sigma^2}\right), \tag{4.1}$$

where h_0 and σ represents the height and width of the ridge, respectively.

Westward-moving modons are very unstable to the topographic forcing. For instance, a short ridge with $h_0 = 0.001$ and $\sigma = 1.0$ can trigger the tilt instability and breaks the modons down. We hereafter do not give any results on the effects of the topography on westward-moving modons. The results in this section and in section 4e are for eastward-moving modons only, with the center of the modons being located initially at $(x, y) = (-5.0, 0)$.

First we give the results with the divergence-vorticity term omitted. For this case, the model used here is similar to Carnevale et al. (1988b) except that the free surface term $F(\partial\psi/\partial t)$ was not considered in their work.

The modon behavior is very complicated depending closely on the height and width of the ridge. In the following, we describe three sets of experiments with different ridge width. In the first set of experiments, we take the width of the ridge $\sigma = 1.0$, which is comparable with the modon size. Eastward-moving modons survive the topographic forcing if the height of the ridge $h_0 \leq 1.28$. If $h_0 > 1.28$, the ridge breaks the modons down except in a window region $1.51 \leq h_0 \leq 1.76$ in which the eastward-moving modons can still survive the topographic perturbation.

Figure 7 shows typical examples where modons survive the topographic forcing. The two vortices are al-

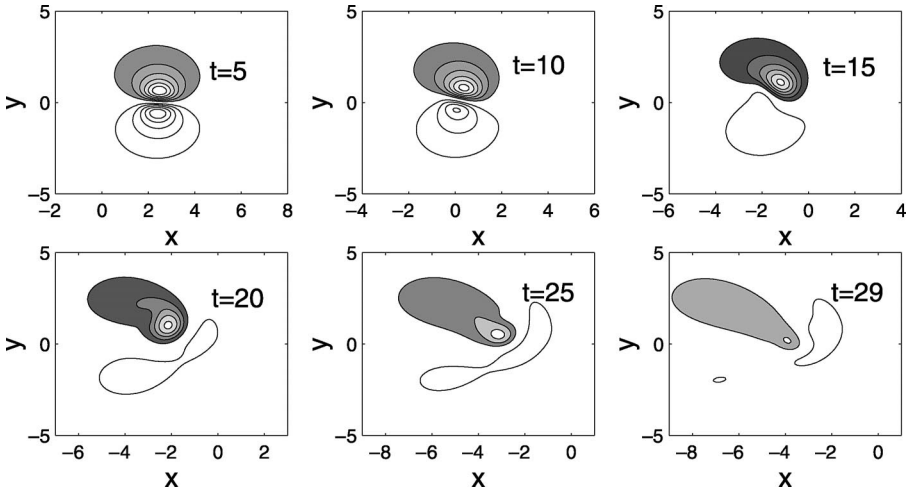

FIG. 6. As in Fig. 5, except $\mu = 0.05$.

ways bounded together as a whole after the modons pass the ridge. The influence of the ridge on the modons is that it perturbs the modons to move in a wavy way. At the location of the ridge the trajectories of the modons form a big trough first, then the modons move downstream in a wavy way with smaller amplitude. The figure also shows that even for the stable case the trajectory of the modon is very sensitive to the height of the ridge; that is, a small difference in the height of the ridge will result in a big difference in the trajectories.

Figure 8 shows a typical case where the ridge breaks the modon down. As the modon moves into the region of the ridge, it begins to move southeastward, and at the time $t = 20$ the modon reaches the lowest latitude, then it turns to the northeast. After $t = 30$, the modon remains almost stationary for a long period of time until its two vortices separate gradually and finally disperse into a wave packet.

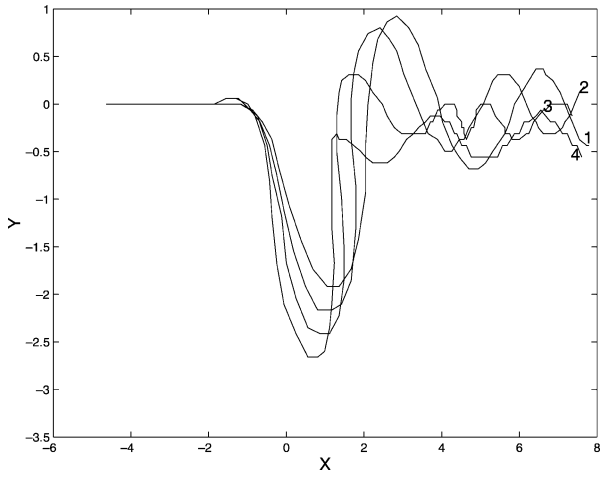

FIG. 7. Stable evolution of an eastward-moving modon that survives the topographic forcing with $\varepsilon = 0$ and $\mu = 0$. The curves are the trajectories of the centers of the modons. The curves 1, 2, 3, and 4 represent the cases where $h_0 = 0.9$, 1.0, 1.1, 1.2, respectively. The modon parameters are $A = 1.0$, $c = 0.4$, $q = 2.121$, and $k = 4.091$.

In the second set of experiments $\sigma = 0.2$, which is a steep-slope case. For this case the eastward-moving modons survive the topographic forcing if $h_0 \leq 1.19$. Like the stable case in the first set of experiments, the eastward-moving modons propagate in an oscillating way after they move out of the ridge. If h_0 satisfies $1.19 < h_0 \leq 1.75$, the modons can still pass through the ridge. After they move out of the ridge, they move very slowly downstream to a place far from the ridge, then they become stationary and retreat and split gradually into two separate vortices and finally break down. If $h_0 > 1.75$, the modons remains stationary for some period of time at a place just downstream of the ridge, then their two vortices separate and break down. If h_0 is much bigger than 1.75, the modons cannot pass through the ridge: when they move into the region of the ridge, their two vortices separate and break down very quickly.

In the third set of experiments $\sigma = 2.5$, which represents a small-slope case. For this case, the critical height of the ridge $h_{0c} = 2.48$, which is much larger than the critical heights in the previous two sets of experiments. The eastward-moving modons survive the topographic forcing if $h_0 \leq h_{0c}$; they break down when $h_0 > h_{0c}$.

Now we describe the topographic effect on the modons with the divergence-vorticity term considered. We here focus our attention only on the case where the width of the ridge $\sigma = 1.0$. It is found that the divergence-vorticity term does alter the modon behavior depending on the Rossby number ε. If ε is very small—see $\varepsilon = 0.001$—the modon behavior is very similar to the case in the first set of experiments above. The critical height of ridge here is still 1.28 as above, but the stable window for this case is $1.38 \leq h_0 \leq 1.75$, which is bigger than the stable window $1.51 \leq h_0 \leq 1.76$ of the first set of experiments above.

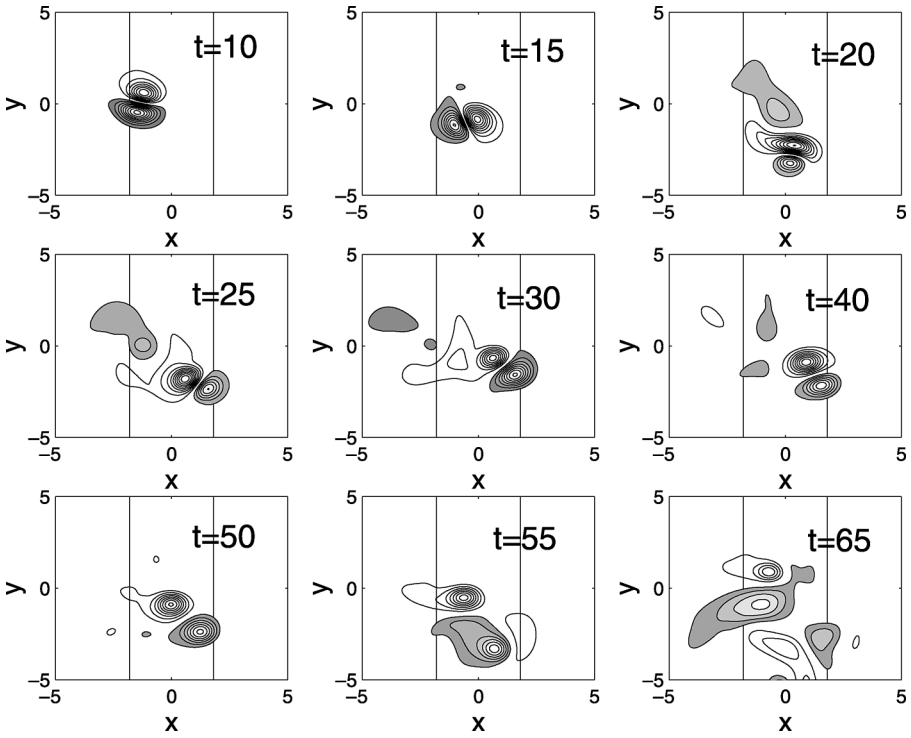

FIG. 8. Unstable evolution of an eastward-moving modon broken down by the topographic forcing with $\varepsilon = 0$, $\mu = 0$, and $h_0 = 1.30$. The curves are the contour lines of the modon streamfunction and the ridge is located between the vertical solid lines. The modon parameters are the same as in Fig. 7.

The modon behavior changes with increasing Rossby number. When $\varepsilon = 0.01$, for example, the critical height of the ridge is $h_{0c} = 1.80$, which is much larger than in the first set of experiments where the critical height is 1.28. Unlike in the first set of experiments above, in the unstable region $h_0 > h_{0c}$ there is no stable window at all for this case. More experiments show that the bigger the ε is, the shorter the critical height is. The critical height is 1.78 when $\varepsilon = 0.02$, while it is 1.65 when $\varepsilon = 0.05$.

d. Combined effects of the surface perturbation and the bottom friction

Perturbed simultaneously by both the surface perturbation term and the bottom friction, term I and term II at the right-hand side of the Eq. (2.8), eastward-moving modons are stable in the sense that they evolve in the same way as in the cases where only the bottom friction is considered. For westward-moving modons, the modon behavior is diverse depending on both the bottom friction parameter μ and the Rossby number ε which represents the strength of the surface term and the nonlinear Ekman effect in the bottom friction. Table 1 gives a set of numerical simulations, where ε and μ vary from 0.01 to 0.05, respectively.

TABLE 1. Evolution of a westward-moving modon perturbed by both the bottom friction and the surface perturbation.

	ϵ				
μ	0.01	0.02	0.03	0.04	0.05
0.01	○	○	○	○	○
0.02	○	○	○	○	○
0.03	○	○	○	○	○
0.04	△	△	△	△	△
0.05	△	△	□	□	□

In this table, the experiments with circles show cases where the surface perturbation term dominates over the bottom friction (Fig. 9 shows a typical example where $\varepsilon = 0.05$ and $\mu = 0.01$). For this case the modon is perturbed to deviate from its initial due-westward motion and moves southwestward. Propagating in this direction, the effect of the β term is opposite to the bottom friction. The β effect would have the modon gaining positive vorticity and thus deepen its cyclone and weaken its anticyclone, but the bottom friction would have the modon decaying asymmetrically with a stronger anticyclone and a weaker cyclone. Under the action of both the β effect and the bottom friction, the modon actually maintains its cyclone unchanged in strength before $t = 20$ and its anticyclone weakens gradually and almost disappears at $t = 20$. Then, the cyclone begins to disperse its energy rightward and become a wave packet and die away gradually.

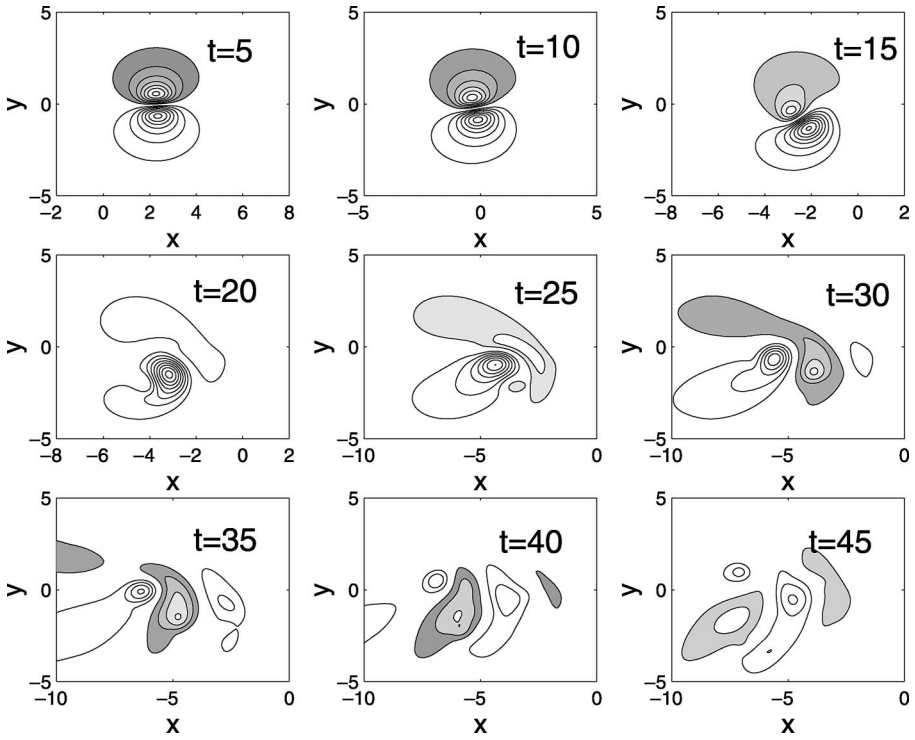

FIG. 9. Unstable evolution of a westward-moving modon perturbed by both the surface perturbation and bottom friction with $\varepsilon = 0.05$ and $\mu = 0.01$. The modon parameters are as in Fig. 3.

For the experiments with triangles in the table, the asymmetric decay of the bottom friction is balanced by the surface perturbation term and the moden still moves westward and its cyclone and anticyclone diminish in time at an approximately equal rate.

For the experiments with squares, the asymmetric decay of the bottom friction dominates over the surface perturbation term. For this case the modon decays in an asymmetrical way. Its cyclone decays much faster than its anticyclone. After the cyclone dies away, the anticyclone also gradually dies away and no wave packet is formed (Fig. 10 shows typical example where $\varepsilon = 0.05$ and $\mu = 0.05$).

e. Combined effects of the surface perturbation, bottom friction, and bottom topography

This section reports numerical results with all the terms—I, II, and III—on the right-hand side of Eq. (2.8) considered.

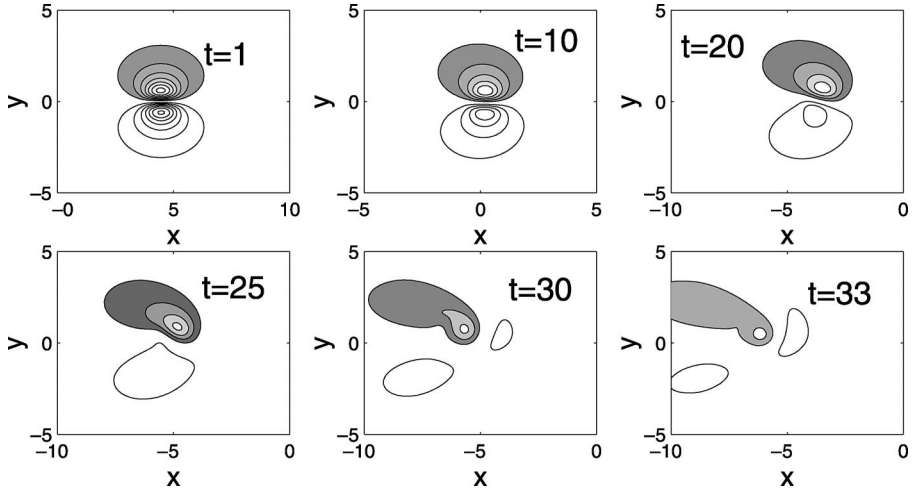

FIG. 10. As in Fig. 9, except $\mu = 0.05$.

TABLE 2. The critical heights of the topography and stable windows within the unstable region for eastward-moving modons perturbed simultaneously by surface term, bottom fiction, and bottom topography.

	ϵ				
μ	0.01	0.02	0.03	0.04	0.05
0.001	$h_{0c} = 1.24$ [1.36, 1.74]	$h_{0c} = 1.27$ [1.35, 1.70]	$h_{0c} = 1.69$	$h_{0c} = 1.65$	$h_{0c} = 1.62$
0.005	$h_{0c} = 1.13$ [1.38, 1.60]	$h_{0c} = 1.12$ [1.35, 1.60]	$h_{0c} = 1.12$ [1.31, 1.58]	$h_{0c} = 1.11$ [1.28, 1.55]	$h_{0c} = 1.11$ [1.25, 1.52]
0.01	$h_{0c} = 0.98$	$h_{0c} = 0.97$ [1.33, 1.34]	$h_{0c} = 0.96$ [1.29, 1.32]	$h_{0c} = 0.95$ [1.26, 1.28]	$h_{0c} = 0.93$

If the bottom friction is strong, modons decay very rapidly before they move into the region of ridge. In order to be able to study the combined effects of the topography, surface perturbation, and bottom friction on modons, we focus our attention on cases where the bottom friction is very weak. We did numerical simulations with $\mu = 0.001$, 0.005, and 0.01, while ε varies from $\varepsilon = 0.01$ to $\varepsilon = 0.05$. Our focus is also limited to the ridge width $\sigma = 1.0$.

Table 2 gives the critical height of the topography and the stable window within the unstable region in which eastward-moving modons still survive the topographic forcing. From the table we see that the critical height varies from case to case depending on both μ, which represents the strength of bottom friction, and ε, which represents the strength of the surface term and nonlinear effects of Ekman pumping in the bottom friction and topographic forcing. Generally the critical height decreases with increasing bottom friction and for fixed μ, it also decreases with increasing ε. The critical height is around 1.25, 1.12, and 0.96 when $\mu = 0.001$, 0.005, and 0.01, respectively.

The stable window within the unstable region occurs irregularly. When $\mu = 0.001$, the window can be observed only with $\varepsilon \leq 0.02$. When $\mu = 0.005$, it always exists. When $\mu = 0.01$, the window exists except where $\varepsilon = 0.01$ and $\varepsilon = 0.05$. The size of the window varies with bottom friction. It decreases with increasing bottom friction. When $\mu = 0.001$, the window size is around 0.38. It is around 0.28 when $\mu = 0.005$. It is only around 0.03 when $\mu = 0.01$.

5. Conclusions and discussions

In this paper the evolution of modons perturbed by the surface term, bottom friction, and bottom topography incorporating nonlinear Ekman pumping is investigated numerically. It is found that both the vorticity-divergence term related nonlinear Ekman pumping and the β effect play an important role in the modon dynamics. Usually the nonlinear Ekman pumping results in asymmetry in the behavior of the two vortices of modons. This asymmetry, along with the β effect, leads to asymmetry in the modon behavior depending on their initial directions of propagation. From the paper the following main conclusions may be reached.

1) The surface term usually perturbs the modons to deviate from their initial direction of propagation. For westward-moving modons, the surface term causes them to move southwestward, and then the tilt instability is triggered due to the β effect. For eastward-moving modons the surface term is not strong enough to trigger the tilt instability, and the modons behave the same way as they are not subject to any perturbation.
2) The bottom friction incorporating nonlinear Ekman pumping causes the modons to decay in asymmetrical way. Their cyclones decay faster than their brothers—the anticyclones. For eastward-moving modons, this asymmetrical decay was counteracted by the vortical change caused by the beta effect, and the two vortices actually decay at approximately the same rate. For westward-moving modons the asymmetrical decay was enhanced by the vortical change caused by the beta effect and the tilt instability is thus triggered out.
3) Perturbed simultaneously by the surface term and bottom friction, eastward-moving modons are stable, while, for westward-moving modons, their behavior is diverse depending on both the strength of the surface perturbation and the bottom friction. If the surface perturbation dominates over the bottom friction, the modons are unstable and they disperse into wave packets. If the bottom friction dominates over the surface perturbation, the modons decay in an asymmetric way, their cyclones decay faster than the anticyclones, and they finally die away early or late with no wave packet formed.
4) Westward-moving modons are always unstable to the topographic forcing. For eastward-moving modons, the topographic effects are complex depending on the height and width of the topography. There is usually a critical height depending on the width of the topography, above which the modons are destroyed, below which the modons can survive the topographic forcing, propagating eastward with their two vortices always bound together. For the case where $\sigma = 1.0$, the modon behavior is more complex: there is a stable window above the critical height, in which modons still survive the topographic forcing even though the ridge is tall. The critical height and the window size decrease with increasing

bottom friction when the surface term, bottom friction, and the nonlinear Ekman pumping effect in the topographic forcing are all included. For this case, the stable window even disappears for some range of parameters.

As pointed out in the introduction, the effects of the bottom friction on modons were studied as early as in McWilliams et al. (1981), Swaters (1985, 1989), and Swaters and Flierl (1989). In these studies, the Ekman pumping used was the classical one, and the decay of the two vortices of the modons caused by the bottom friction is therefore symmetrical, and so the modon behavior has nothing to do with the direction of their propagation. In contrast, in our work here, the Ekman pumping is nonlinear and the bottom friction corresponding to this kind of pumping results in asymmetrical decay of the two vortices of the modons. This asymmetrical decay of the vortices along with the β effect leads to asymmetrical modon behavior depending on the initial direction of propagation.

The effects of the bottom friction incorporating nonlinear Ekman pumping on vortices were also studied in Zavala Sansón and van Heijst (2000) and Zavala Sansón et al. (2001). The former study used an f plane (unlike our β plane) but still found an asymmetrical decay of monopoles with different signs of vorticity. Zavala Sansón et al. (2001) studied the effects of bottom friction on an eastward-moving modon (called Chaplygin–Lamb dipoles in their article), again on an f plane. They showed that the dipole decays asymmetrically: cyclone damping faster than its anticyclone, and it veers southeastward, which differs from the picture of the viscous evolution of eastward-moving modons on a β plane reported here. In our work, eastward-moving modons subject to bottom friction incorporating nonlinear Ekman pumping still propagate eastward initially with a diminishing amplitude and velocity, but eventually their direction of propagation is *reversed.* Apparently this difference is caused by the beta effect, which causes the modon to gain positive vorticity and thus reduces the difference in the strength of the two vortices caused by the dissipation of bottom friction.

Though Zavala Sansón et al. (2001) did not give numerical results in their paper on the effects of the bottom friction incorporating nonlinear Ekman pumping on a westward-moving modon, we can imagine that the dipole will be forced to move northwestward due to the asymmetrical decay of the two vortices and then die away gradually, which is obviously different from the behavior of bottom-friction-perturbed westward-moving modons in our work. This difference is also caused by the β effect.

It is also interesting to note that the picture reported here of the unstable evolution of topographically perturbed eastward-moving modons is obviously different from that of Carnevale et al. (1988b) where the cyclones are usually captured by the topography while the anticyclones travel southwestward after the instability occurs. For our case, after the instability occurs, the two vortices of the modons separate gradually, then disperse into wave packets. The instability may occur at the ridge, or just downstream of the ridge, or far away from the topography, depending on the width and height of the undersea ridge. Another significant phenomenon in our case studies is that there is a window of stability within the interval of ridge height for which the modons are unstable—in other words, the onset of the instability is not a monotonic function of width height. The stability window was not seen Carnevale et al. (1988b). These differences may be caused by the upper free surface, which was omitted in Carnevale et al. (1988b).

Acknowledgments. The authors are grateful for the comments and suggestions from the reviewers. This work was supported by the Chinese NSF Grant 40275012, the National Key Basic Research Project G1998040907, and Grant OCE9986368 (with a supplement from the International Programs Office) from the U. S. NSF. The main part of the work was done when the first author, B. Tan, was visiting the AOSS department at the University of Michigan. He is grateful to the support from the department.

REFERENCES

Araki, K., S. Toh, and T. Kawahara, 1998: Stability of a modon structure: Multipole expansion analysis. *Wave Motion,* **28,** 69–78.

Boyd, J. P., 1981: Analytical approximations to the modon dispersion relation. *Dyn. Atmos. Oceans,* **6,** 97–101.

——, 2001: *Chebyshev and Fourier Spectral Methods.* 2d ed. Dover Publications, 668 pp.

Butchart, N., K. Haines, and J. C. Marshall, 1989: A theoretical and diagnostic study of solitary waves and atmospheric blocking. *J. Atmos. Sci.,* **46,** 2036–2078.

Carnevale, G. F., M. Briscolini, and R. Purini, 1988a: Numerical experiments on modon stability to topographic perturbations. *Phys. Fluids,* **31,** 2562–2566.

——, G. K. Vallis, and R. Purini, 1988b: Propagation of barotropic modons over topography. *Geophys. Astrophys. Fluid Dyn.,* **41,** 45–101.

Flierl, G. R., V. D. Larichev, J. C. McWilliams, and G. M. Reznik, 1980: The dynamics of baroclinic and barotropic solitary eddies. *Dyn. Atmos. Oceans,* **5,** 1–41.

Gordin, A., and V. I. Petviashvili, 1985: Lyapunov-stable quasigeostrophic vortices. *Sov. Phys. Dokl.,* **30,** 1004–1006.

Hesthaven, J. S., J. P. Lynov, and J. Nycander, 1993: Dynamics of non-stationary dipole vortices. *Phys. Fluids,* **4A,** 467–476.

Hobson, D. D., 1991: A point vortex dipole model of an isolated modon. *Phys. Fluids,* **5A,** 3027–3033.

Holton, J. R., 1979: *An Introduction to Dynamic Meteorology.* 2d ed. Academic Press, 391 pp.

Jovanovic, D., and W. Horton, 1993: Stability of drift-wave modons in the presence of temperature gradients. *Phys. Fluids,* **5B,** 9–18.

Laedke, E. W., and K. H. Spatsckek, 1986: Two dimensional drift vortices and their stability. *Phys. Fluids,* **29,** 33–142.

Larichev, V. D., and G. M. Reznik, 1976: Two-dimensional solitary Rossby waves. *Dokl. Akad. Nauk SSSR,* **2331,** 1077–1079.

Makino, M., T. Kamimura, and T. Taniuti, 1981: Dynamics of two

dimensional solitary vortices in a low-β plasma with convective motion. *J. Phys. Soc. Japan,* **50,** 980–989.
McWilliams, J. C., 1980: An application of equivalent modons to atmospheric blocking. *Dyn. Atmos. Oceans,* **5,** 43–66.
——, and N. J. Zabusky, 1982: Interactions of isolated vortices. *Geophys. Astrophys. Fluid Dyn.,* **19,** 207–227.
——, G. R. Flierl, V. D. Larichev, and G. M. Reznik, 1981: Numerical studies of barotropic modons. *Dyn. Atmos. Oceans,* **5,** 219–238.
Nezlin, M. V., and E. N. Snezhkin, 1993: *Rossby Vortices, Spiral Structures, Solitons.* Springer-Verlag, 223 pp.
Nycander, J., 1992: Refutation of stability proofs for dipole vortices. *Phys. Fluids,* **4A,** 467–476.
Pedlosky, J., 1987: *Geophysical Fluid Dynamics.* 2d ed. Springer-Verlag, 710 pp.
Sakuma, H., and M. Ghil, 1990: Stability of stationary barotropic modons by Lyapunov's direct method. *J. Fluid Mech.,* **211,** 393–416.
Swaters, G. E., 1985: Ekman layer dissipation in an eastward traveling modon. *J. Phys. Oceanogr.,* **15,** 1212–1216.
——, 1986a: Stability of conditions and a priori estimates for equivalent barotropic modons. *Phys. Fluids,* **29,** 1419–1422.
——, 1986b: Barotropic modon propagation over slowly varying topography. *Geophys. Astrophys. Fluid Dyn.,* **36,** 85–113.
——, 1989: A perturbation theory for the solitary drift-vortex solutions of the Hasegawa–Mima equation. *J. Plasma Phys.,* **41,** 523–539.
——, and G. K. Flierl, 1989: Ekman layer dissipation of a barotropic modon. *Mesoscale/Synoptic Coherent Structures in Geophysical Turbulence,* J. C. J. Nihoul and B. M. Jamart, Eds., Elsevier Press, 149–165.
Tan, B., 2000: Ekman pumping for stratified planetary boundary layers adjacent to a free surface or topography. *J. Atmos. Sci.,* **57,** 3334–3336.
Wu, Y., and M. Mu, 1999: Nonlinear instability of dipole vortices and atmospheric blocking. *Prog. Natl. Sci.,* **9,** 234–237.
Zabusky, N. Y., and J. C. McWilliams, 1982: A modulated point-vortex model for geostrophic β-plane dynamics. *Phys. Fluids,* **25,** 2175–2182.
Zavala Sansón, L., and G. J. F. van Heijst, 2000: Nonlinear Ekman effects in rotating barotropic flows. *J. Fluid Mech.,* **412,** 75–91.
——, ——, and J. J. J. Doorschoot, 1999: Reflection of barotropic vortices from a step-like topography. *Nuovo Cimento,* **22,** 909–929.
——, ——, and N. A. Backx, 2001: Ekman decay of a dipolar vortex in a rotating fluid. *Phys. Fluids,* **13,** 440–451.